



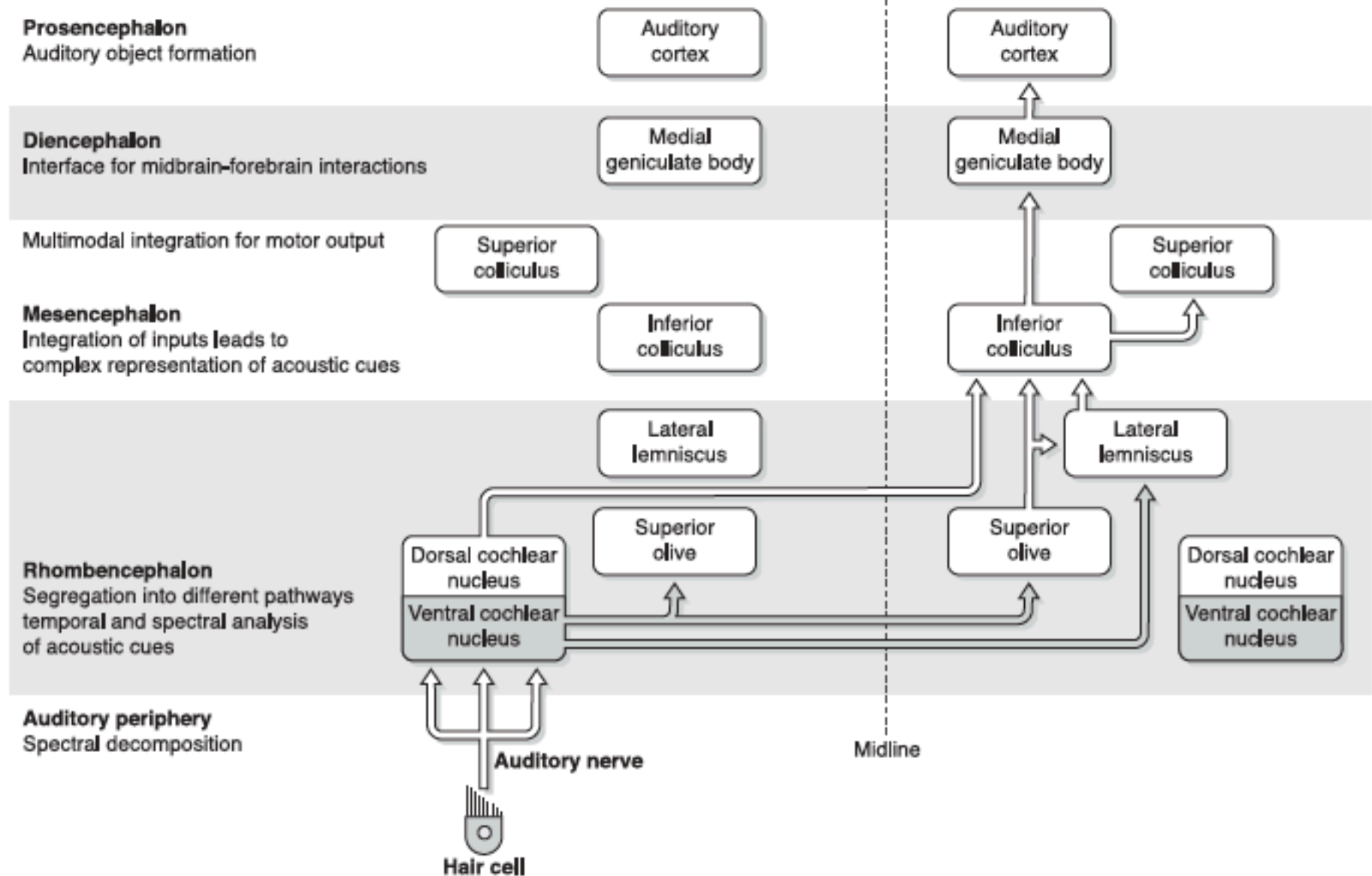
580.422


System Bioengineering II: Neurosciences

**Central Auditory System (1)**

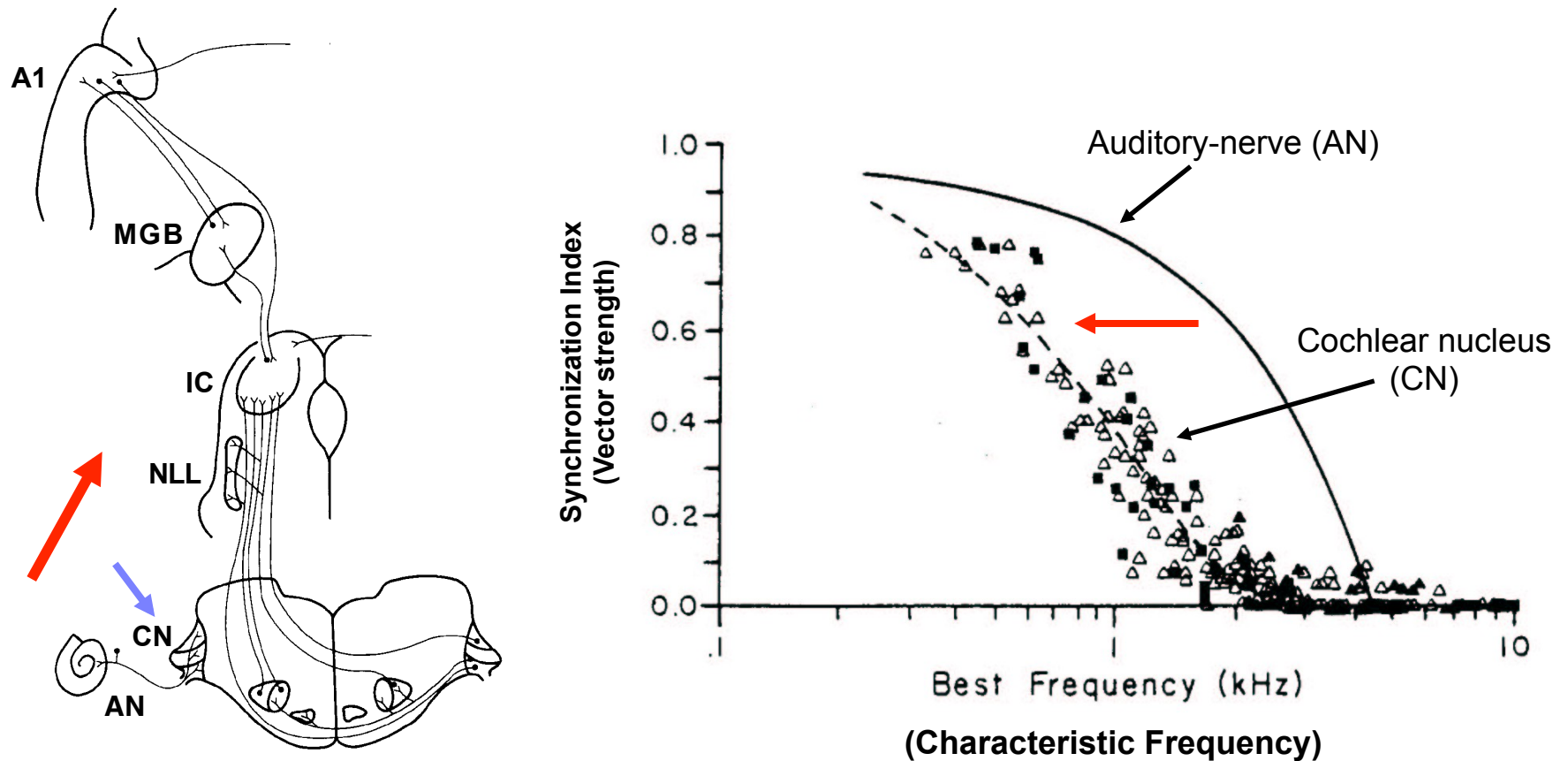
Prof. Xiaoqin Wang

## The mammalian ascending auditory pathway



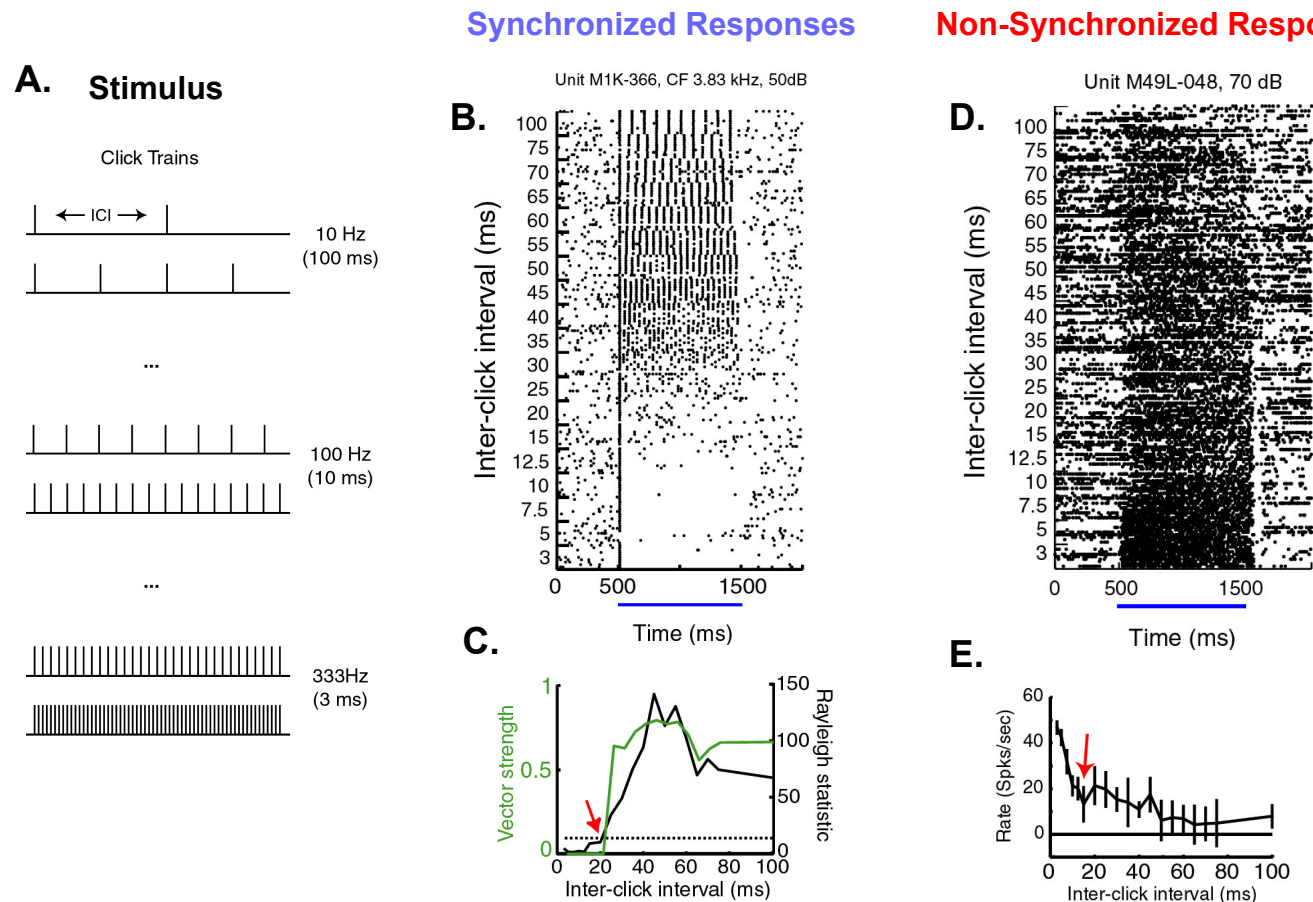
- 
- 1) CNS neurons can extract (compute) stimulus information not explicitly encoded by sensory receptors.
  - 2) CNS transforms isomorphic (faithful) representations of sensory stimuli to non-isomorphic representations

## Phase-locking is degraded at higher processing centers



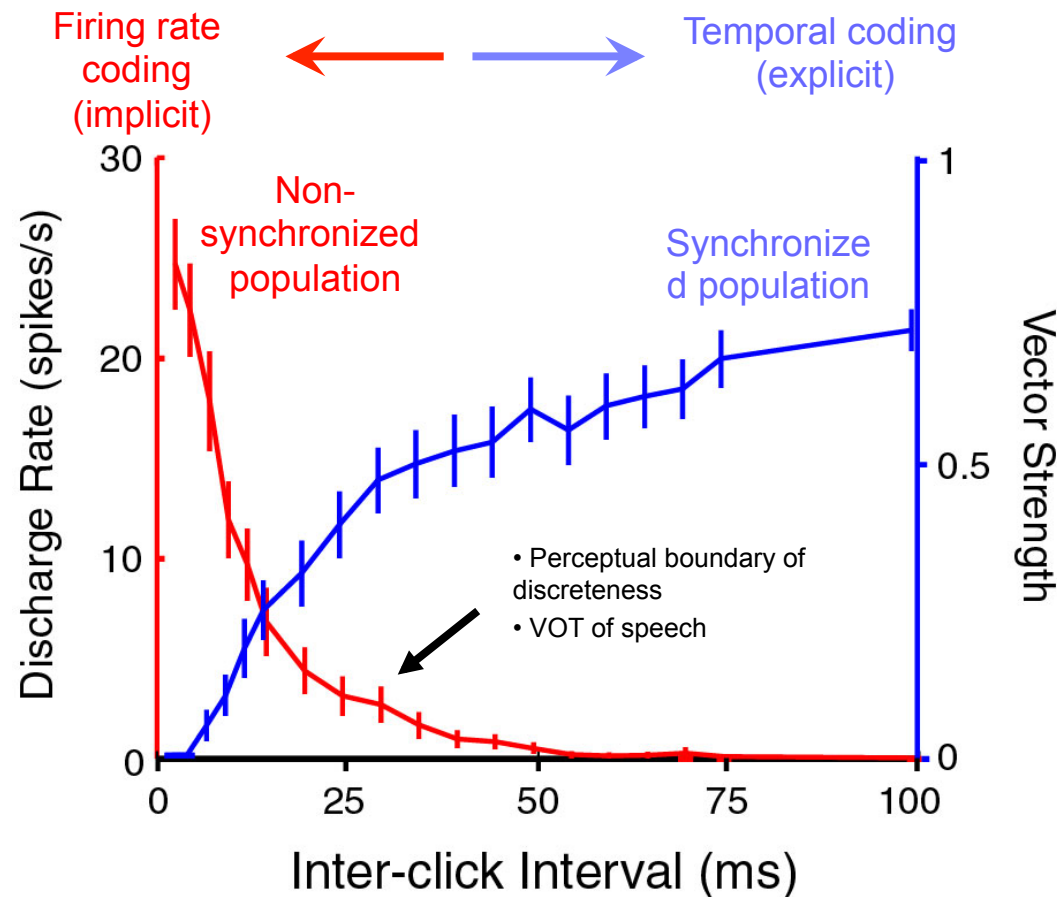
The amount of “phase-locking” in neural firing can be quantified by *synchronization index* or *vector strength*. For auditory nerves (AN), the amount of phase-locking is a function of a neuron’s best frequency (also called characteristic frequency) as shown by the solid curve (from Johnson 1980). In the cochlear nucleus (CN), the next auditory processing station (see illustration of ascending auditory pathway on the left), the amount of phase-locking decreases at high frequency as shown by the data points and a dashed curve fit to the data (from Blackburn and Sachs 1990). This trend (illustrated by red arrows in both left and right figures) continues throughout the ascending auditory pathway.

# Two types of neurons in auditory cortex in response to repetitive stimuli



**A:** Acoustic stimuli used in these experiments were sequences of clicks (brief sounds) with various inter-click intervals (ICI). **B:** An example of neurons in auditory cortex that respond to the click train stimuli with phase-locking discharges when ICI is long (“*synchronized response*”), but stop responding when ICI is short. **C:** Vector strength (dashed line) and Rayleigh statistics (solid line) are used to quantify stimulus synchronized responses shown in **A**. The dotted line (at the Rayleigh statistics of 13.8) indicates the threshold for statistically significant stimulus-synchronized activity ( $p < 0.001$ ). **D:** An example of neurons in auditory cortex that only respond to the click train stimuli when ICI is short, but without phase-locking discharges (“*non-synchronized response*”). **E:** Mean firing rate is plotted versus ICI for the non-synchronized response shown in **D**. (From Lu, Liang and Wang, *Nature Neuroscience* 2001).

## Auditory cortex transforms rapid time-varying signals into firing-rate based representations



Auditory cortex uses a temporal (timing) code to represent slowly varying signals and a firing-rate based code to represent rapidly varying signals. A combination of temporal and firing-rate representations can encode a wide range of inter-click-intervals (ICI) in auditory cortex. Blue curve is the vector strength averaged from 36 neurons that have stimulus synchronized discharges in response to click train stimuli. Red curve is the mean firing rate averaged from 50 neurons that show non-synchronized discharges to click train stimuli. (From Lu, Liang and Wang, *Nature Neuroscience* 2001).

\_\_\_\_\_

## The first central processing station in ascending auditory pathway

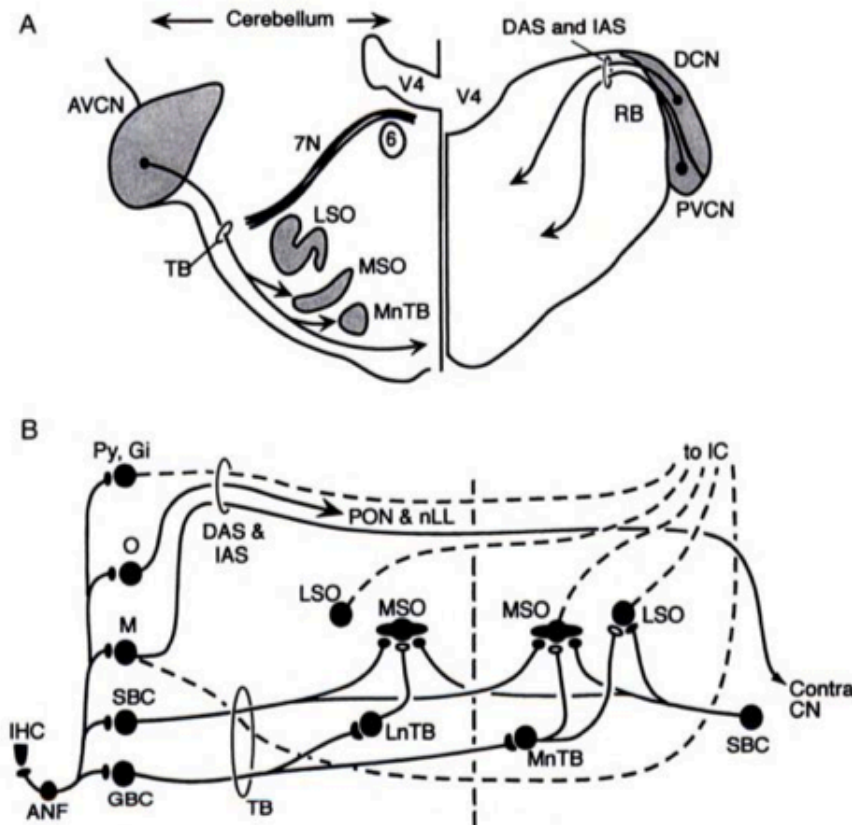


Fig. 4.3. Ascending pathways from the cochlear nucleus through the brainstem. **A:** The cat brain-stem is shown in frontal-plane cross sections: the left half section is at the level of the anteroventral cochlear nucleus (AVCN) and superior olive; the right half section is slightly caudal, at the level of the dorsal (DCN) and posteroventral (PVCN) cochlear nuclei. The auditory nerve enters the nucleus between these two planes of section. Output fibers from the cochlear nucleus pass through the trapezoid body *TB* and dorsal and intermediate acoustic striae *DAS* and *IAS* (shown as arrows). Other abbreviations: *V4*, fourth ventricle; *6*, abducens nerve nucleus; *7N*, seventh (facial) nerve. **B:** Some of the cochlear nuclear principal cell types with their projections to the nuclei of the superior olivary complex and the inferior colliculus (*IC*). The auditory pathway begins with the transducer cell, the inner hair cell (*IHC*). Auditory nerve fibers (*ANF*) carry action potentials from the inner ear to the cochlear nucleus. From the VCN, bushy cells (*SBC* and *GBC*) innervate the medial (*MSO*) and lateral (*LSO*) superior olivary nuclei. The innervation is bilateral, with symmetrical connections on the two sides, only some of which are shown (the midline of the brain-stem is shown by the dashed vertical line). The *GBCs* form large calyceal synapses on principal cells of the medial nucleus of the trapezoid body (*MnTB*) that in turn provide glycinergic inhibition to *MSO* and *LSO* principal cells. Neurons of the lateral nucleus of the trapezoid body (*LnTB*) are also inhibitory and project to the *MSO* as well as projecting back to the cochlear nucleus (not shown). T-multipolar cells (*M*, dashed line) in the VCN project through the *TB*, and pyramidal (*Py*) and giant (*Gi*) cells from the *DCN* project through the *DAS* to the contralateral *IC*; D-multipolar cells (*M*-solid line) project to the contralateral cochlear nucleus. Octopus cells (*O*) project from the VCN via the *IAS* to the contralateral superior paraolivary nucleus (*PON*) and to the ventral nucleus of the lateral lemniscus (*nLL*; neither is shown).



# Sound Localization by Human Listeners

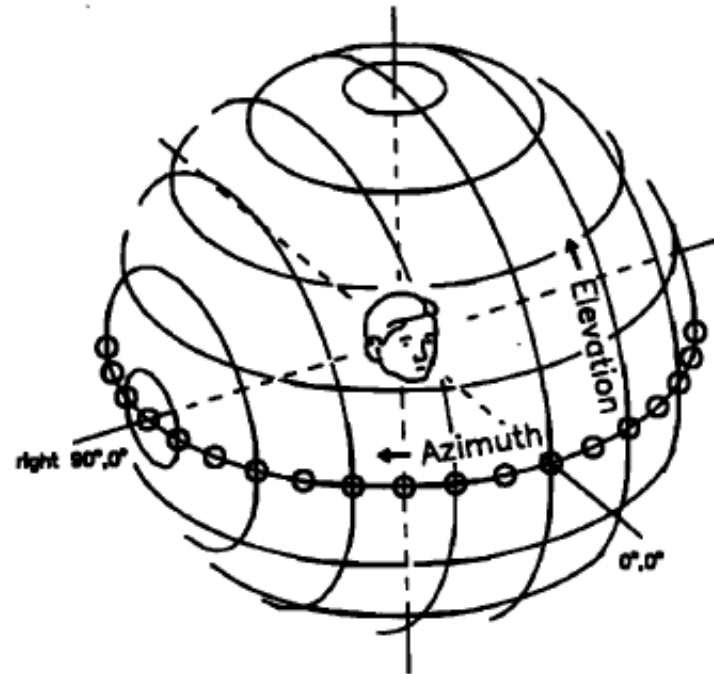


FIG. 2. The spatial coordinate system. The subject is represented in the center of the coordinate sphere; the viewpoint is from  $30^\circ$  to the subject's right and  $30^\circ$  above the horizontal plane. Isoazimuth and isoelevation lines are drawn in  $20^\circ$  increments. The small circles separated by  $10^\circ$  along the horizontal plane represent loudspeakers mounted on a moveable hoop of radius 1.2 m. The axis of rotation of the hoop coincided with the interaural axis of the subject. Rotations of the hoop about this axis produced changes in elevation, whereas changes in the speaker that was activated produced changes in azimuth (from Middlebrooks *et al.*, 1989).



# Sound Localization by Human Listeners

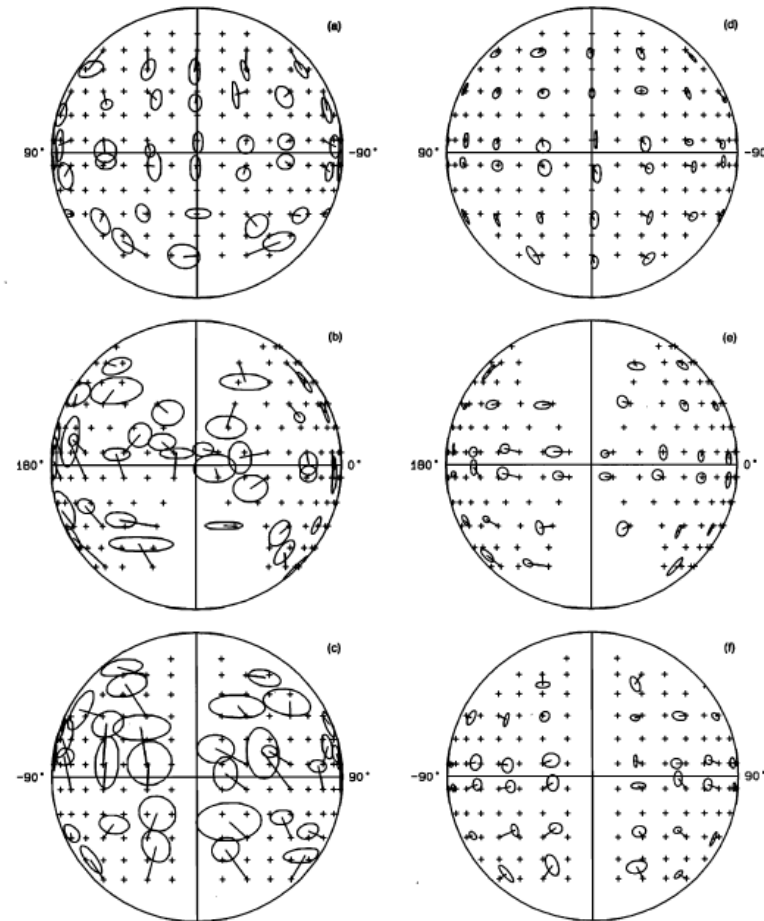


FIG. 3. Open-loop (left) and closed-loop (right) localization performance. Results for subject 1 are drawn on the coordinate sphere as if looking in at the subject from [(a) and (d)] in front, from [(b) and (e)] the right, or from [(c) and (f)] the rear. All stimulus locations, separated by  $10^\circ$  of azimuth and elevation, are represented by small crosses. For clarity, results are shown only at  $20^\circ$  intervals. The vectors connect the stimulus locations with the locations of the mean responses of six trials. Thus the horizontal and vertical components of each vector represent the signed errors in the horizontal and vertical dimensions, respectively. The horizontal and vertical axes of the corresponding ellipses represent  $\pm 1$  s.d. about the mean responses. The vectors and ellipses follow the surface of the coordinate sphere; therefore, they are foreshortened near the edges of each plot. Front/back confusions have been screened out, as discussed in the text.

# Sound Localization Cues

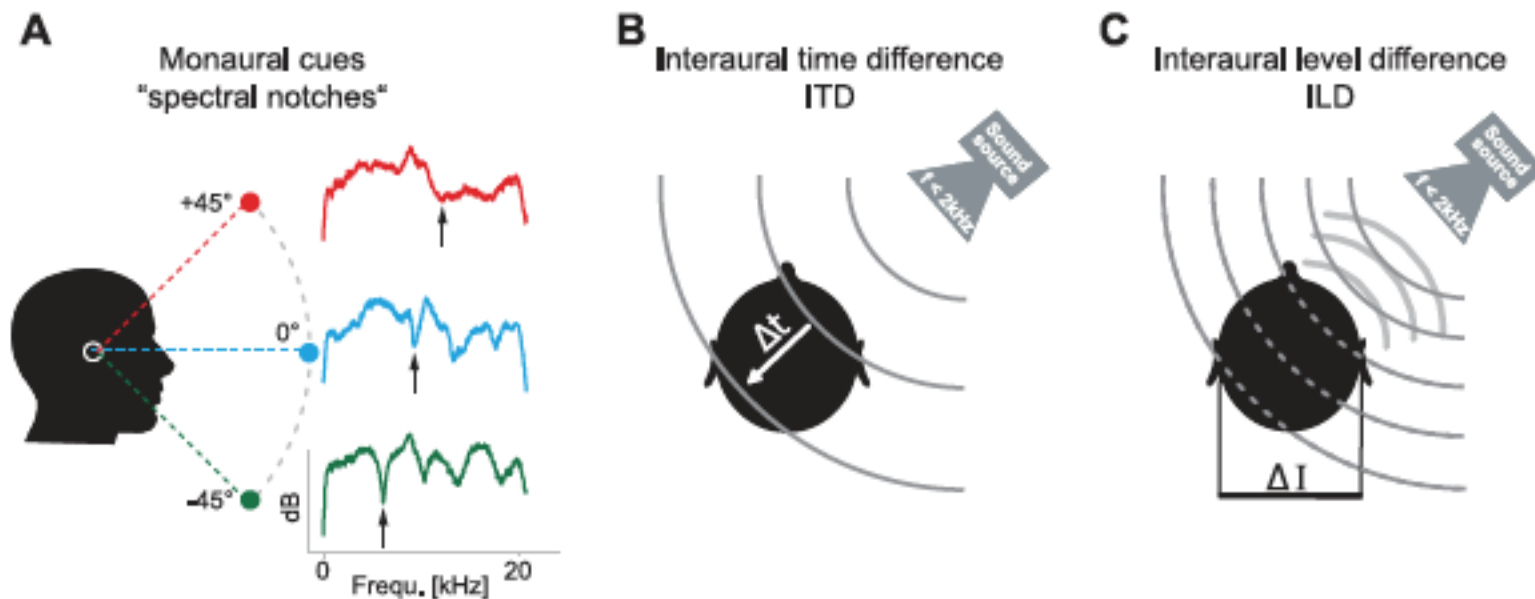
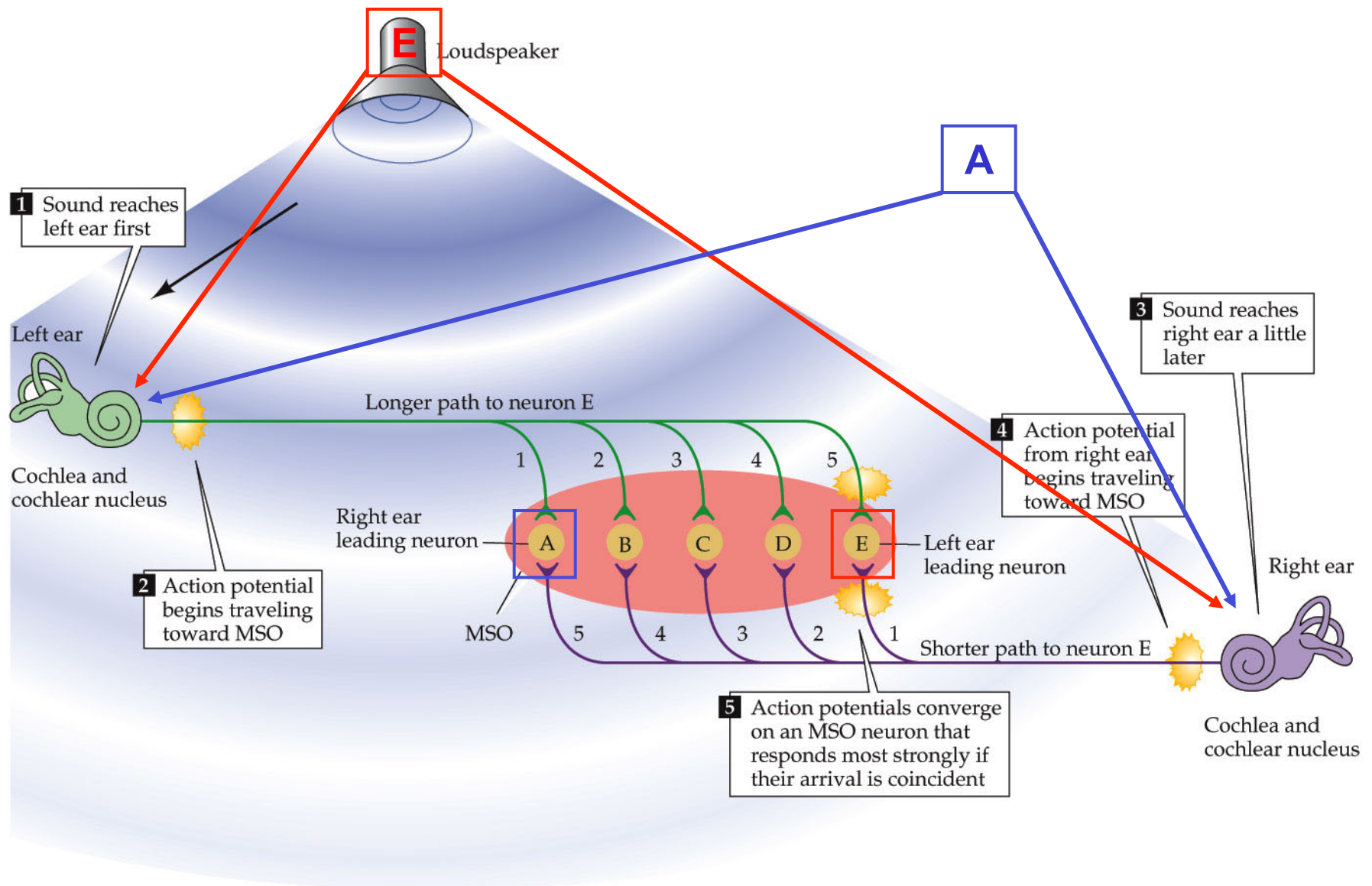


FIG. 2. Cues for sound localization. *A*: spectral analysis as a monaural cue for sound localization in the vertical plane. Interaction of a broadband sound with the head and, primarily, the outer ear alters the effective spectrum of the sound impinging on the eardrum in a manner dependent on the location of the sound source in the vertical plane. Most prominently, the central notch (black arrows) in the effective spectrum of the sound shifts to higher frequencies when the sound source is shifted from below ( $-45^\circ$ , green) to above the horizon ( $+45^\circ$ , red). The spectra shown are digitally computed from 1-s white noise stimuli (cutoff frequency, 44.1 kHz) convolved with KEMAR head-related impulse responses and averaged over 50 repetitions. *B*: interaural time differences (ITD): the difference in the arrival time ( $\Delta t$ ) of a sound wave (gray lines) at the two ears is used to localize a sound source in the horizontal plane. For frequencies below  $\sim 2$  kHz, information in the fine structure of the sounds is available for ITD processing. *C*: interaural level differences (ILD): for frequencies higher than  $\sim 2$  kHz, the shadowing effect of the head creates increasingly sizable differences in the intensity of the sounds at the two ears ( $\Delta I$ ) that are utilized for sound localization in the horizontal plane.

Figure 13.13 How the MSO computes the location of a sound by interaural time differences



## ITD Computation via “Delayed Lines” (Birds)

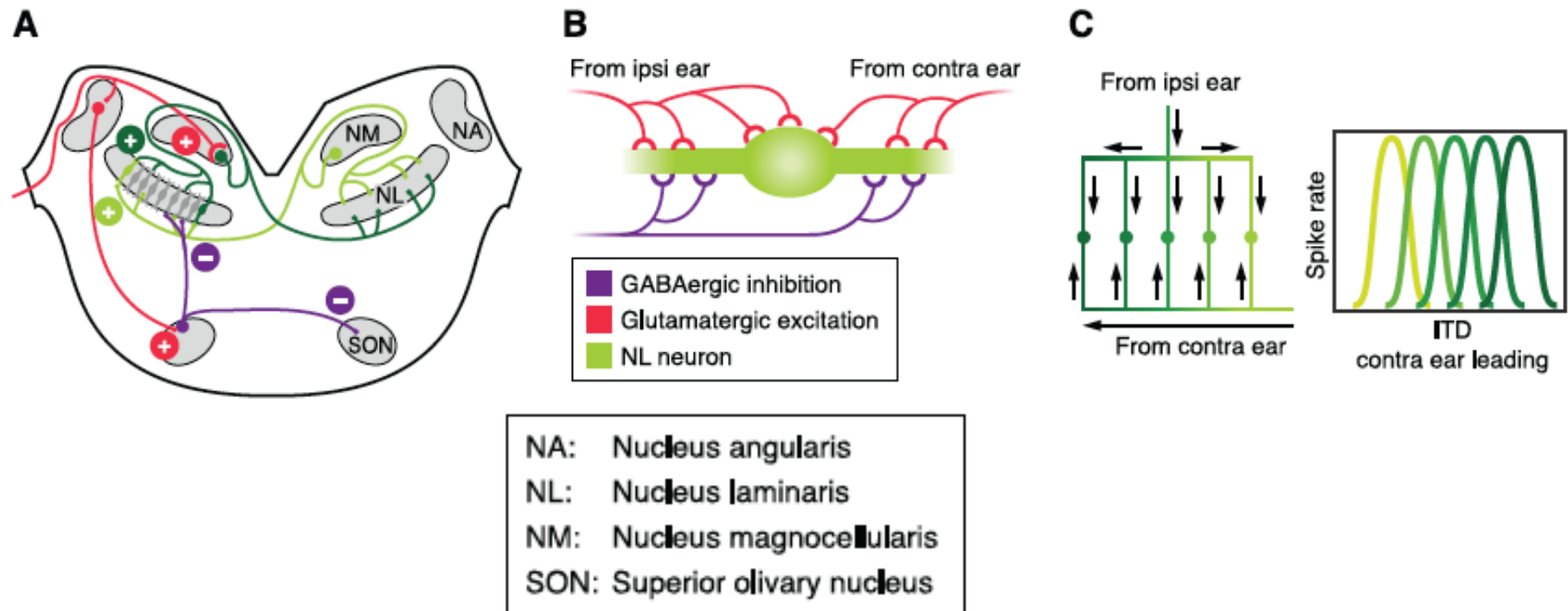


FIG. 7. The neuronal basis underlying ITD processing in birds. *A*: schematic of the avian ITD circuit [for the chick, modified from Burger et al. (23)]. Coincidence-detector neurons in the NL are aligned in a thin horizontal lamina, innervated bilaterally by excitatory inputs from the NM. The axons of NM neurons are bifurcated, one branch projecting to the contralateral NL and the other to the ipsilateral. Only the contralateral projection is arranged in the form of an array of delay lines. GABAergic input to the NL is provided by the ipsilateral SON. *B*: schematic of the distribution of binaural excitatory (red) and monaural inhibitory (blue) input to a NL neuron (green). Depicted are somatic and dendritic areas of a NL principal cell. *C*: delay-line arrangement of binaural inputs (vertical lines in *left panel*) to NL neurons (closed circles in *left panel*). Note that contralateral inputs systematically increase in axon length along the horizontal axis, giving rise to a gradient in preferred ITD (see *right panel*; ITD functions are color coded according to their position along the delay axis in the *left panel*).



# ITD Computation via “Excitation-Inhibition” (Mammals)

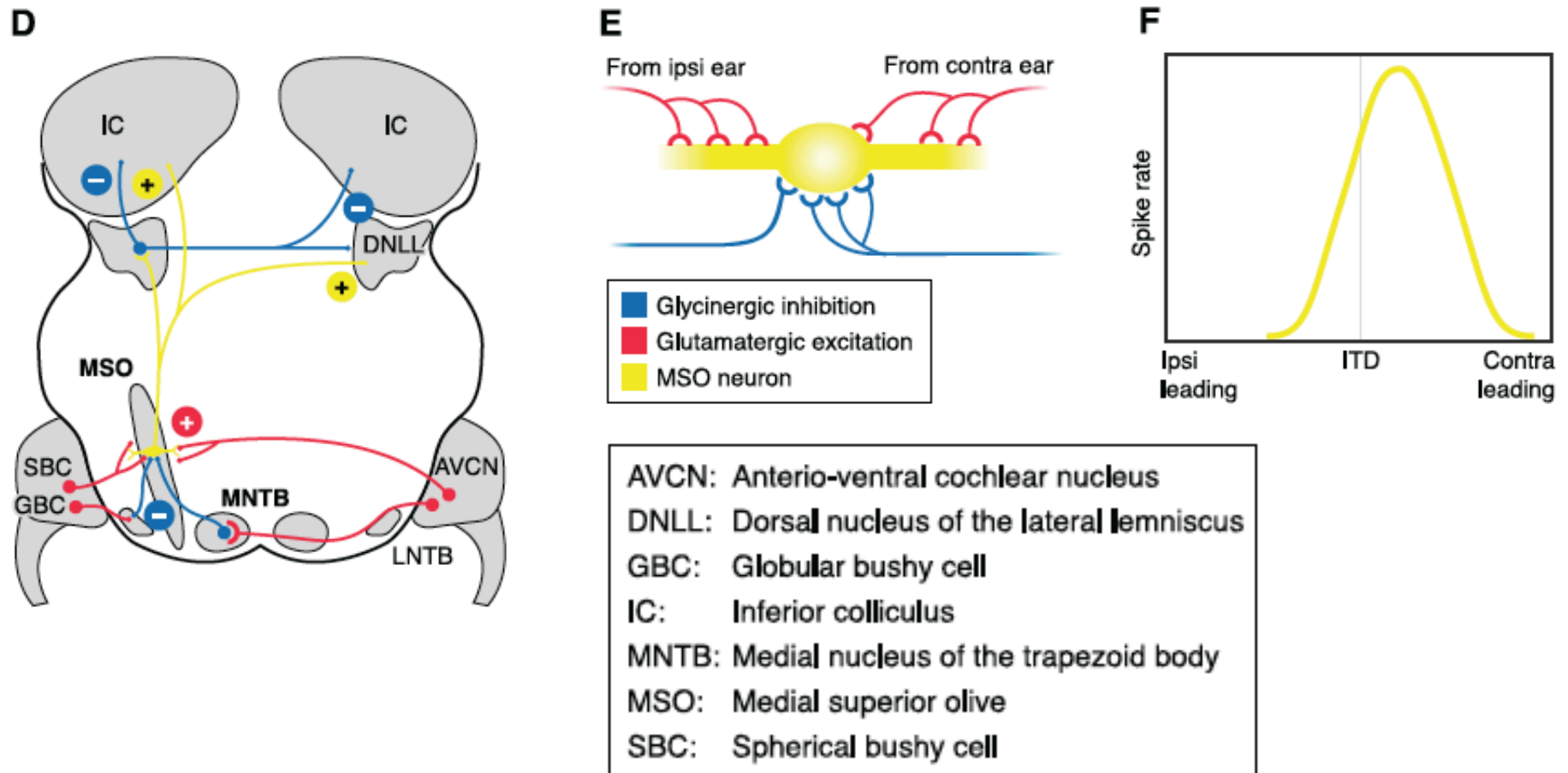
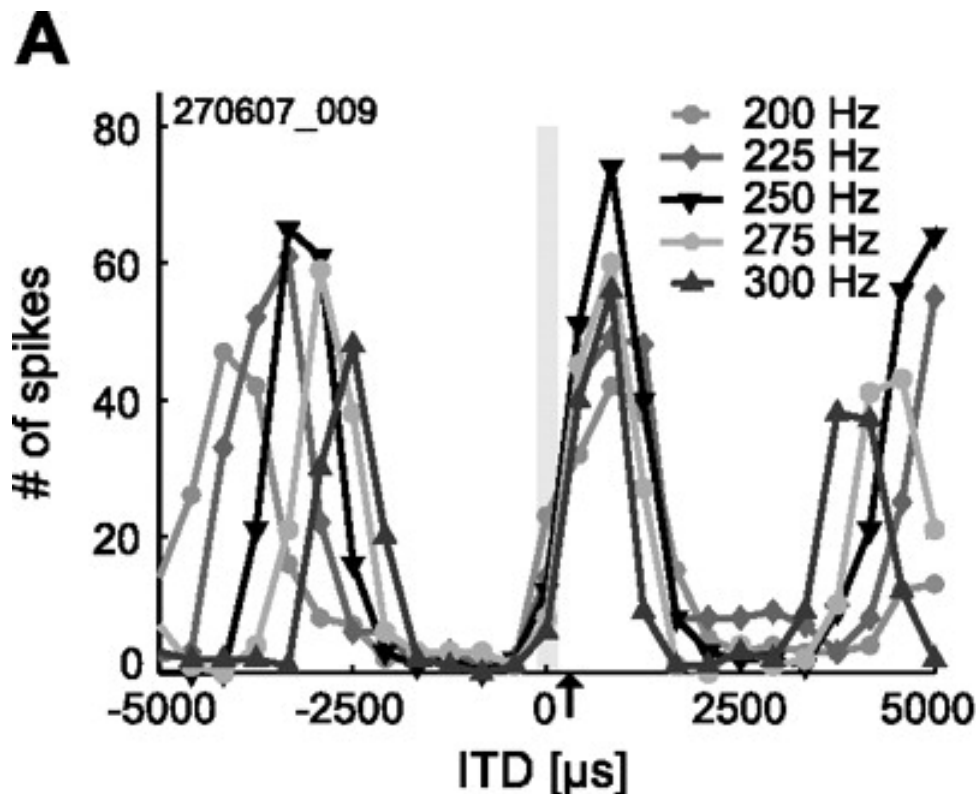


FIG. 8. The neuronal basis underlying ITD processing in mammals. *A*: drawing by Ramon y Cajal (1907, Ref. 190) depicting input pattern to (from left to right) LSO and MSO as well as calyces of Held terminating in the MNTB. *B*: drawing by Ramon y Cajal (1907, Ref. 190) depicting MSO principal cells (dark black) extending dendrites in a bipolar fashion. *C*: confocal picture of a section through adult gerbil MSO. Staining for glycine receptors (yellow) is restricted to somatic areas of MSO neurons. Dendrites (blue, MAP2 staining) are mostly devoid of glycine receptors. *D*: schematic of the mammalian ITD circuit. MSO principal cells (yellow) receive binaural excitatory inputs (red) from SBCs in the ipsilateral and contralateral AVCN as well as binaural inhibitory inputs (blue) from the LNTB and MNTB. MSO neurons send excitatory projections to the DNLL and IC. *E*: schematic of binaural excitatory (red) and binaural inhibitory (blue) synaptic input distribution onto a MSO neuron (yellow). Depicted are somatic and dendritic areas of a MSO principal cell. *F*: schematic of typical ITD function for a MSO neuron.

Grothe et al. (2010)

## Examples of neural responses to ITD at five different frequencies recorded from the gerbil MSO



Characteristic delay (CD) and characteristic phase (CP). *A*: example recording of ITD functions from a neuron in the gerbil MSO for five different sound frequencies. When presented with frequencies below or above the BF of the cell (250 Hz), the maximal response rate and dynamic range decreased. The CD of the neuron (238 s) is denoted by the arrow. [Modified from Pecka et al. (2008)]

# Two Mechanisms for ITD Computation

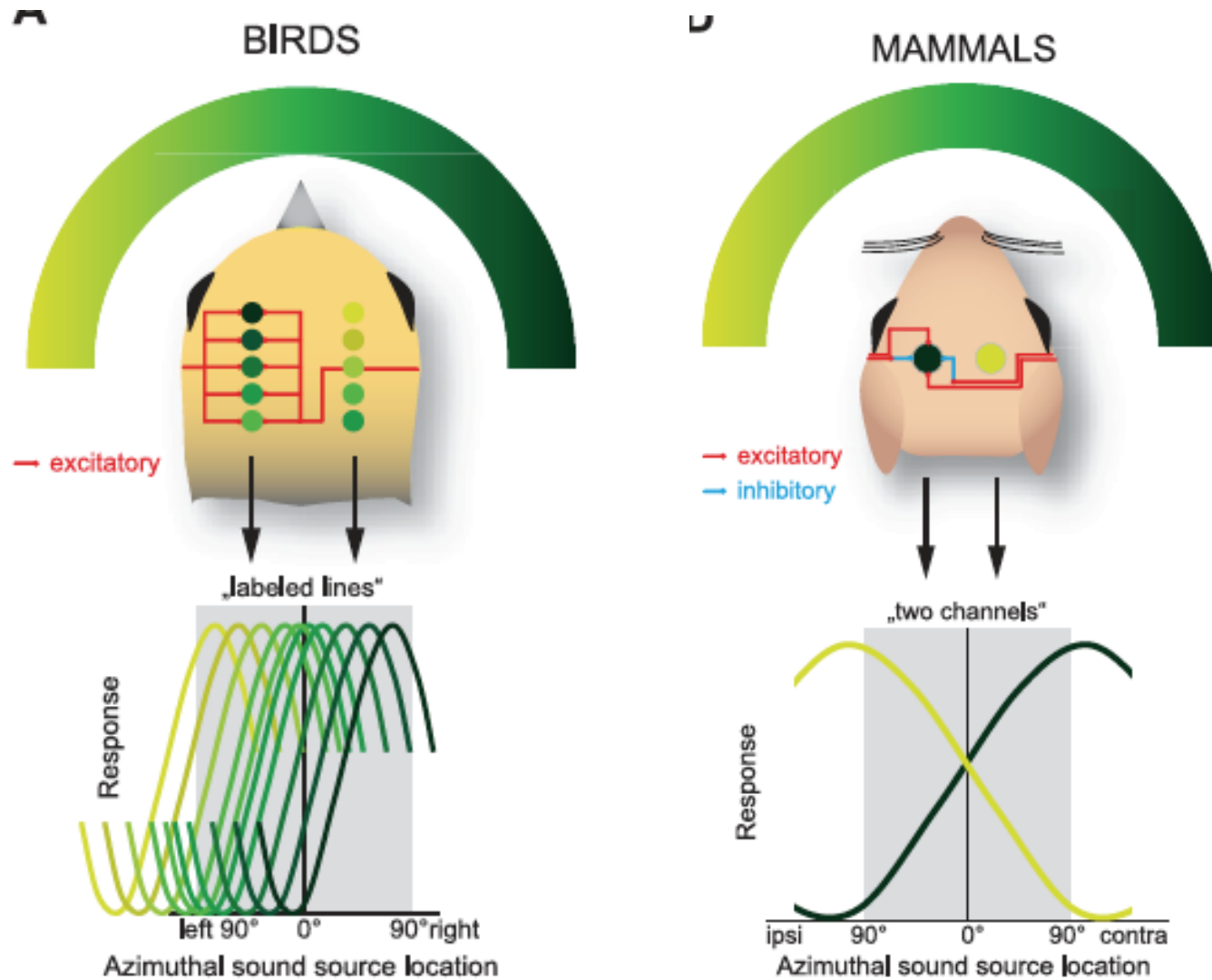
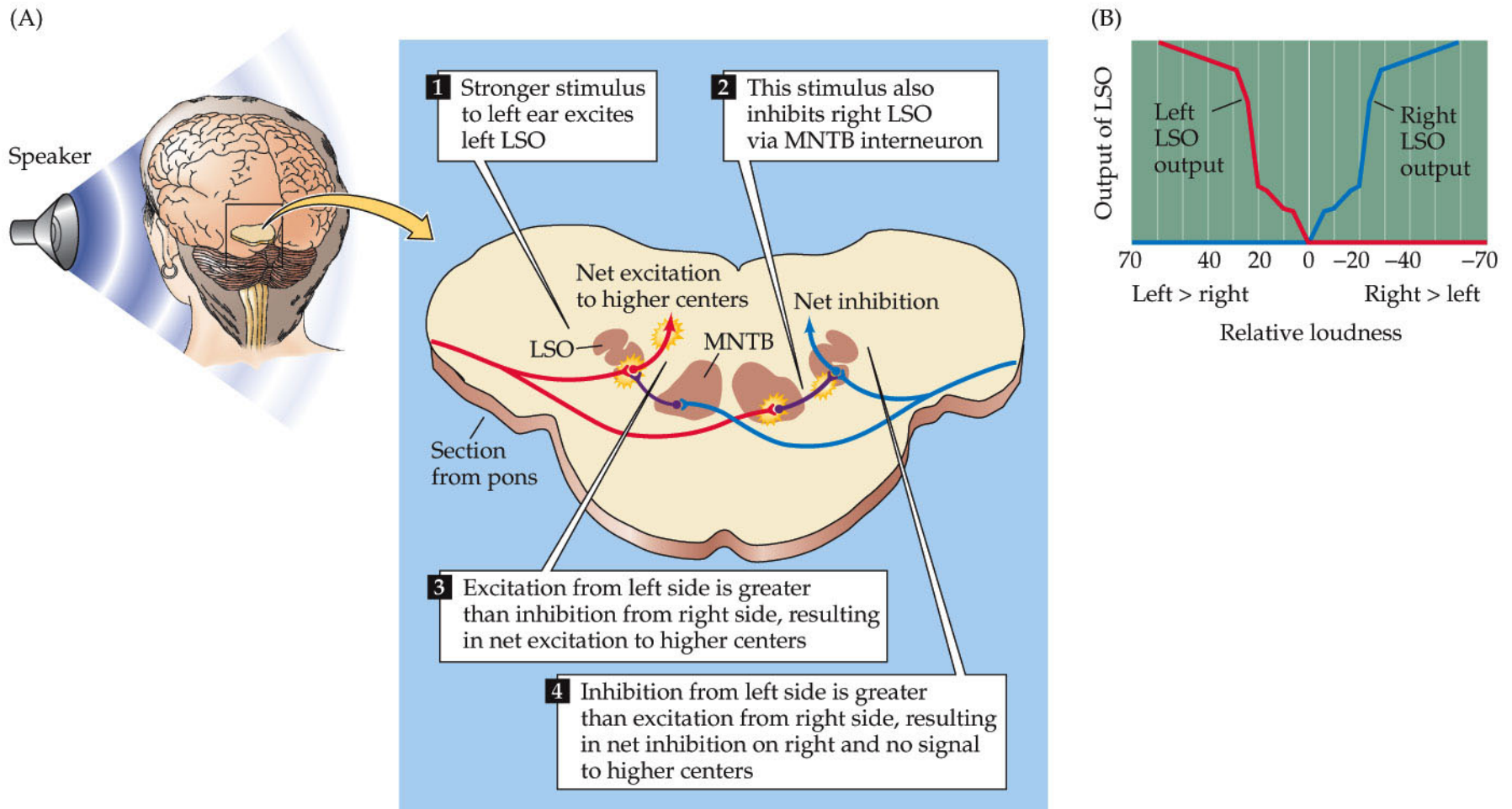




Figure 13.14 LSO neurons encode sound location through interaural intensity differences



# ILD Computation via “Excitation-Inhibition”

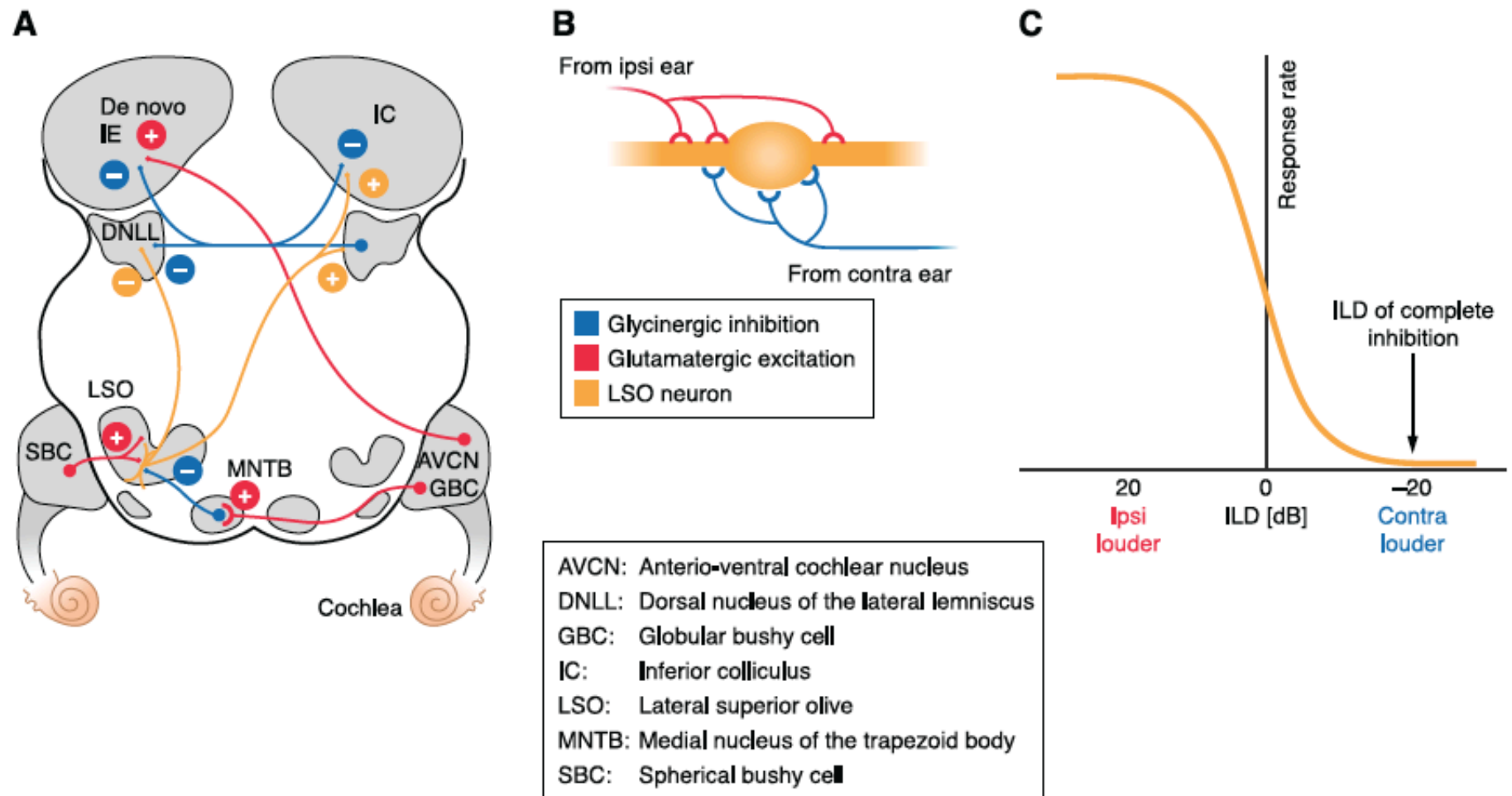
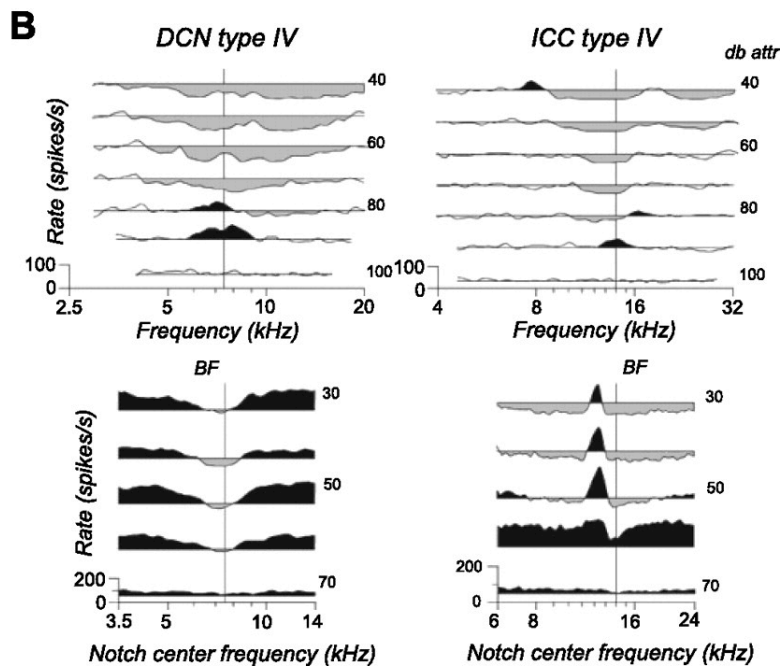
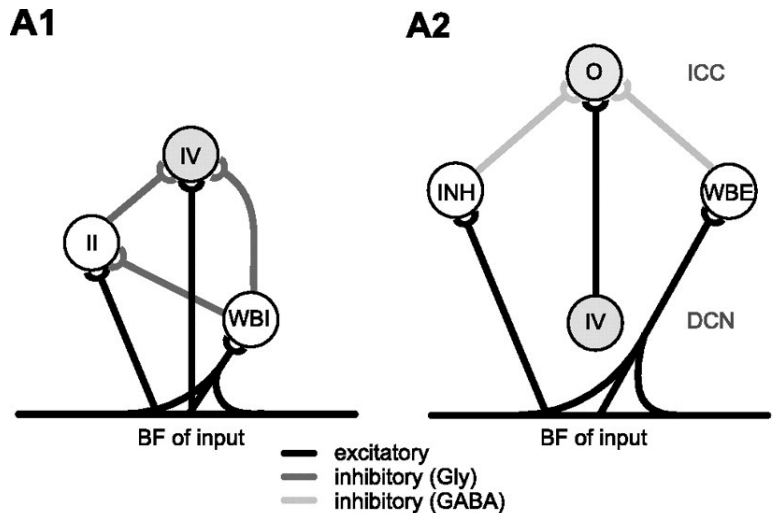


FIG. 6. The neuronal basis underlying ILD processing. **A**: schematic of the mammalian ILD circuit. ILD sensitivity is first created in the LSO by convergence of excitatory inputs from SBCs located in the ipsilateral AVCN and inhibitory inputs from ipsilateral MNTB, which is itself innervated by GBCs of the contralateral AVCN. Projections of the LSO to the contralateral DNLL and IC are excitatory and inhibitory to the ipsilateral DNLL and IC. In the IC, ILD sensitivity is created de novo by the convergence of monaural contralateral excitatory input from the AVCN and binaural inhibitory input from the DNLL. **B**: schematic of the distribution of excitatory (red) and inhibitory (blue) input onto a LSO neuron (orange). Depicted are somatic and dendritic areas of a LSO principal cell. **C**: schematic of the typical sigmoid ILD function of a LSO neuron is shown.

# The neuronal basis for analysis of spectral cues



The neuronal basis for analysis of spectral cues. *A*: hypothetical model of circuits involved in spectral analysis at the level of the DCN (*A1*) and the IC (*A2*). Horizontal line at the bottom indicates array of tonotopic inputs to DCN/IC. II, type II unit; IV, type IV unit; INH, inhibitory input with below-BF frequency tuning; O, prototypic type O unit; WBE, wide band excitatory input; WBI, wide band inhibitory input. [*A1* modified from Nelken and Young (1994); *A2* modified from Davis et al. (2003).] *B*: response maps of a DCN type IV unit (*left column*) and an IC type O unit (*right column*) to pure tones (*top panels*) and notched noise (*bottom panels*). Gray regions depict excitatory discharge rates, and black regions indicate inhibitory discharge rates (relative to spontaneous rates, indicated by horizontal lines). [From Davis et al. (2003).]



## **Suggested readings:**

- 1) “*Neuroscience*” textbook, Chapter 13: The auditory system
- 2) Grothe B, Pecka M, McAlpine D. Mechanisms of sound localization in mammals. *Physiol Rev.* 2010 Jul; 90(3): 983-1012.